

Quantum machines using Cu_3 -like compounds modeled by Heisenberg antiferromagnetic in a triangular ring

Onofre Rojas¹ and Moises Rojas¹

¹*Department of Physics, Institute of Natural Science,
Federal University of Lavras, 37200-900 Lavras-MG, Brazil*

A theoretical study of an antiferromagnetically coupled spin system, specifically $\text{Cu}_3 - \text{X}$ ($\text{X}=\text{As}, \text{Sb}$), characterized by a slightly distorted equilateral triangle configuration is presented. Using the Heisenberg model with exchange and Dzyaloshinskii-Moriya interactions, g-factors, and an external magnetic field, three quantum machines are investigated using this system as the working substance, assuming reversible processes. For $\text{Cu}_3 - \text{X}$ the magnetocaloric effect (MCE) is significant at low temperatures (around 1K) under a perpendicular magnetic field ($\sim 5\text{T}$). Although only the $\text{Cu}_3 - \text{As}$ compound is considered, since the $\text{Cu}_3 - \text{Sb}$ compound behaves quite similarly. How MCE influences the Carnot machine, which operates as a heat engine or refrigerator when varying the external magnetic field is analyzed. In contrast, the Otto and Stirling machines can operate as heat engines, refrigerators, heaters, or thermal accelerators, depending on the magnetic field intensity. The results indicate that enhanced MCE broadens the operating regions for these machines, with the Otto and Stirling machines primarily functioning as refrigerators and accelerators. The corresponding thermal efficiencies are also discussed for all operating modes.

I. INTRODUCTION

In the past two decades, significant efforts have been made to explore thermodynamic processes where quantum features of matter are crucial. This research has successfully combined theoretical proposals [1] with experimental evidence [2], bridging the gap between quantum thermodynamics concepts and practical applications. Quantum heat engines, like Carnot and Otto, have been studied, with their characteristics compared to classical counterparts. Additionally, a quantum heat engine model has been analyzed for efficiency and irreversibility [3, 4]. Studies on entangled quantum heat engines have provided insights into how entanglement influences thermodynamic efficiency, reinforcing the second law [5, 6]. Quantum thermodynamics offers a framework for understanding and optimizing engines and refrigerators [7]. The study of quantum heat engines based on harmonic oscillators has enhanced our understanding of optimization and irreversibility [8, 9]. Experiments with quantum-dot heat engines, which operate without mechanical parts, have shown near-ideal efficiency, highlighting their relevance to future quantum technologies [10]. Moreover, research on quantum thermal machines in coupled double quantum dots has revealed various operational regimes [11].

Recent investigations have advanced quantum Carnot, Otto, and Stirling engines, surpassing previous limitations in achieving Carnot efficiency with quantum and nanoscale heat engines. These include achieving Carnot efficiency through semi-local thermal operations with dual bath interactions [12]. A six-stroke irreversible quantum Carnot cycle showed inner friction significantly reduces work output and efficiency [13]. Classical magnetic Otto cycles outperformed quantum ones in work extraction due to thermodynamic equilibrium [14]. Energy quantization effects in the Otto cycle were found to

enhance performance, with experimental proposals using trapped ions [15]. The reversible quantum Stirling cycle, involving single or coupled spin systems, revealed conditions under which a heat engine transforms into a refrigerator [16]. Comparisons between quantum Stirling and Otto cycles for interacting spins highlighted the Stirling cycle's superiority in work and operational range [17]. A quantum Stirling engine based on dinuclear metal complexes offered tunable modes, with applications in emerging quantum technologies [18]. Several works have explored theoretical dimer systems as working substances, including quantum engines, refrigerators, and heaters within a quantum Otto cycle with coupled spins [19–22], and including Dzyaloshinskii–Moriya interactions [23]. Though single-spin and spin lattice systems have been extensively studied [24, 25], trimer systems have been rarely explored, with one notable quantum Otto cycle analysis [26].

On the other hand, nanoscale materials with Giant Magnetocaloric Effect (GMCE) are highly valued for their excellent surface-to-volume ratio, intensified interactions, and rapid thermal responses, making them ideal for temperature regulation. Applications include a room-temperature thermal diode [27], a self-pumping magnetic cooling device using Mn-Zn ferrite nanoparticles for energy conservation without external power [28], and a ferrofluid-based magnetic cooling system for efficient heat transfer [29]. Additionally, ferrofluid droplets in microfluidic environments [30] and magnetostructural phase transitions in Ni-Mn-Ga films with notable MCE at low fields [31] have been explored. Other applications involve energy conversion with gadolinium thick films [32, 33], magnetic hyperthermia treatments [34], and enhancing drug delivery via nanocarriers [35].

The study of magnetic materials is crucial for advancements in spintronics, nanoscale fabrication, and medical applications. Research on a Cu_3 nanomagnet has uncovered phenomena such as half-step magnetization, hys-

teresis loops, and asymmetric magnetization, attributed to adiabatic changes and Dzyaloshinskii-Moriya interactions (DMI) [36]. Spin-electric coupling has also been explored [37]. Investigations into $S = 1/2$ spin triangle clusters show that their magnetization and spin configurations are influenced by diamagnetic heteroatoms ($X = \text{As}$ and Sb) [38], highlighting their potential in spin-based quantum gates [39]. Studies on spin-frustrated trinuclear copper complexes with triaminoguanidine revealed strong antiferromagnetic interactions with minimal antisymmetric exchange [40], along with research on various triangular copper structures [41–45]. $S = 1/2$ antiferromagnetic triangular spin rings are promising for studying unique quantum magnetization effects, such as unusual magnetization jumps in spin-frustrated $(\text{VO})_3^{6+}$ -triangle-sandwiched octadecatungstates, which show atypical magnetization steps [46]. The antisymmetric exchange in a tri-copper(II) complex has clarified its origins and theoretical implications, advancing electronic structure calculations [47].

Theoretical investigations into nanomagnets or magnetic molecular clusters, which extend beyond experimental observations, are crucial. Extensive research has documented these insights, with notable theoretical explorations highlighted in the literature [48–51]. Recent studies on the V_6 polyoxovanadate molecular magnet [48] used numerical methods to reveal its adaptable magnetocaloric properties. Another study examined the spin-1/2 Hamiltonian in coupled isosceles Heisenberg triangles via exact diagonalization, detailing the quantum phase transition diagram, magnetization at zero temperature, and thermodynamic behavior [50]. Further investigation into a Cu_5 pentameric molecule using the spin-1/2 Heisenberg model clarified its thermodynamic characteristics, phase transitions, magnetization, and magnetocaloric effects [51]. Karlova et al. explored antiferromagnetic spin-1/2 XXZ Heisenberg clusters, revealing additional magnetization plateaus and an enhanced magnetocaloric effect near magnetization shifts [49].

In our study, we focus on the $\text{Cu}_3 - X$ ($X = \text{As}, \text{Sb}$) configuration, with its isosceles triangular structure. Previous research by Choi et al. [36, 38, 39] shows that this configuration fits the Heisenberg model due to its triangular framework. The study of MCE in Cu_3 -like spin systems has clarified their fundamental properties, particularly at low temperatures [52]. This paper is structured as follows: Sec. 2 covers the thermodynamics of the model and quantum machines. Sec. 3 examines the Carnot machine, Sec. 4 analyzes the Otto machine, and Sec. 5 discusses the Stirling engine. We conclude with our findings in Sec. 6.

II. THERMODYNAMICS OF THE MODEL

To investigate quantum thermodynamics for machine applications, we analyze the energy levels of a spin Hamiltonian relevant to Cu_3 -like systems, using the

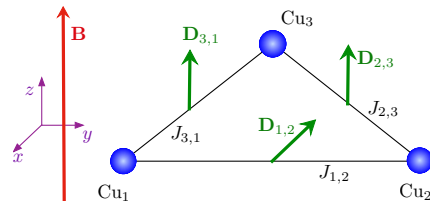


Figure 1. Schematic representation of the Cu_3 -like system, where the triangle lies in the xy -plane.

Table I. Magnetic parameters of the $\{\text{Cu}_3 - X\}$ compounds adjusted to experimental data in units of Kelvin, where X denotes either As or Sb, as extracted from Ref. [38].

Parameters	$\{\text{Cu}_3 - \text{As}\}$	$\{\text{Cu}_3 - \text{Sb}\}$
$J_{1,2}^x = J_{1,2}^y$	4.50 K	4.49 K
$J_{1,2}^z$	4.56 K	4.54 K
$J_{2,3}^x = J_{2,3}^y = J_{3,1}^x = J_{3,1}^y$	4.03 K	3.91 K
$J_{2,3}^z = J_{3,1}^z$	4.06 K	3.96 K
$D_{1,2}^z = D_{2,3}^z = D_{3,1}^z$	0.529 K	0.517 K
$D_{1,2}^x = D_{1,2}^y$	0.529 K	0.517 K
$g_1^x = g_1^y$	2.25	2.24
$g_2^x = g_2^y$	2.10	2.11
$g_3^x = g_3^y$	2.40	2.40
$g_1^z = g_2^z = g_3^z$	2.06	2.07

Heisenberg model in an isosceles triangular spin ring context[36, 38, 39]. This study builds on previous work that characterizes the Hamiltonian of $\text{Cu}_3 - X$ compounds [36, 38, 39]. The Hamiltonian is expressed as

$$\mathbf{H} = \sum_{j=1}^3 \sum_{\alpha=x,y,z} J_{j,j+1}^{\alpha} S_j^{\alpha} S_{j+1}^{\alpha} + \sum_{j=1}^3 \left[\mathbf{D}_{j,j+1} \cdot (\mathbf{S}_j \times \mathbf{S}_{j+1}) + \mu_B \mathbf{S}_j \cdot \mathbf{g}_j \cdot \mathbf{B}_j \right], \quad (1)$$

where $J_{j,j+1}^{\alpha}$ represents the exchange interaction parameters between sites j and $j+1$ for $\alpha = \{x, y, z\}$. The vector $\mathbf{D}_{j,j+1} = (D_{j,j+1}^x, D_{j,j+1}^y, D_{j,j+1}^z)$ represents the Dzyaloshinskii-Moriya interaction, while $\mathbf{g}_j = (g_j^x, g_j^y, g_j^z)$ are the site-dependent g -factors. The magnetic field \mathbf{B} is assumed to be site-independent on the triangle, and μ_B is the Bohr magneton. Parameters were derived from Electron Spin Resonance (ESR) data [36, 38, 39], shown in table I. Only $\mathbf{D}_{1,2} = (D, D, D)$ is isotropic, while $\mathbf{D}_{2,3}$ and $\mathbf{D}_{3,1}$ contribute only to the z -component, $\mathbf{D}_{2,3} = \mathbf{D}_{3,1} = (0, 0, D)$. A schematic view of the Cu_3 -like system is illustrated in Fig.1.

For convenience, the Hamiltonian (1) is expressed in Kelvin (K) units, redefining μ_B as $\hat{\mu}_B = \frac{\mu_B}{k_B} = 0.6717156644\text{K/T}$, where k_B denotes the Boltzmann constant, thereby simplifying the measurements of the magnetic field \mathbf{B} in Tesla (T) units. This conversion implies all subsequent units are in terms of k_B .

The eigenvalues of the Hamiltonian (1) are obtained through numerical diagonalization, essential for under-

standing the energy spectrum of the system under a fixed magnetic field.

Therefore, the partition function can symbolically be represented by

$$\mathcal{Z}(T, B) = \text{tr} \left(e^{-\mathbf{H}/T} \right) = \sum_{i=1}^8 e^{-\varepsilon_i(B)/T}, \quad (2)$$

where the eigenvalues $\varepsilon_i(B)$ depend of the Hamiltonian parameters given in table I, external magnetic field \mathbf{B} (in Tesla), and the temperature T (in Kelvin). Although any physical quantity can be derived from \mathcal{Z} , the eigenvalues must be obtained numerically, limiting analytical solutions. This result, relevant to quantum machines, highlights the importance of understanding magnetic and thermodynamic properties at the quantum level, crucial for advancing quantum technologies.

A. Internal energy, entropy, heat and work

Here we consider the Cu₃-like compound, which has a finite number of energy levels given by eq.(1). In order to explore quantum machine, we need to express the average internal energy as follows:

$$U(T, B) = \sum_{i=1}^8 \varepsilon_i p_i. \quad (3)$$

here p_i is the distribution probability for i -th energy level, which depends implicitly of magnetic field B and temperature T , as well as ε_i depends implicitly of magnetic field B .

In quantum thermodynamics, the first law of thermodynamics is expressed as

$$dU = dQ + dW, \quad (4)$$

where $dQ = TdS$, with entropy given by

$$\mathcal{S}(T, B) = -k_B \sum_{i=1}^8 p_i \ln(p_i), \quad (5)$$

Therefore, we can express dQ as

$$dQ = \sum_{i=1}^8 \varepsilon_i dp_i, \quad (6)$$

whereas dW becomes

$$dW = \sum_{i=1}^8 p_i d\varepsilon_i. \quad (7)$$

B. Quantum reversible process

Work is related to changes in energy levels ε_i and results from varying an external parameter like the magnetic field B . In a Cu₃-like system, the quantum isothermal process involves adjusting the magnetic field, energy

gaps, and occupation probabilities to keep equilibrium with the heat bath. In the quantum isochoric process, no work is done; heat transfers between temperatures while occupation probabilities p_i and entropy \mathcal{S} adjust to reach thermal equilibrium. The quantum adiabatic process keeps population distributions constant ($dp_i = 0$) with no heat exchange ($dQ = 0$), although work can still occur [53].

1. Conditions for operational modes of a quantum machine

Adjusting the cycle parameters can reverse the total work done, in line with the second law of thermodynamics. In a heat engine, the system absorbs heat from a hot reservoir at T_h ($Q_{in} > 0$) and releases it into a cooler reservoir at T_l ($Q_{out} < 0$), converting part of this heat into work ($W_{net} > 0$). For a refrigerator, heat is transferred from the cooler reservoir at T_l to the hotter one at T_h , with the system absorbing heat from T_l ($Q_{out} > 0$) and releasing it at T_h ($Q_{in} < 0$), requiring more work input than output ($W_{net} < 0$). An accelerator uses work ($W_{net} < 0$) to enhance heat flow from T_h to T_l ($Q_{in} > 0$ and $Q_{out} < 0$). A heater uses work ($W_{net} < 0$) to produce heat in both reservoirs, causing heat release in both ($Q_{in} < 0$ and $Q_{out} < 0$).

Table II. Characteristic of work and heat allowed by the second law of thermodynamics. The signal (+) means work done by the system and heat absorbed; (-) means work done on the system and heat released.

Operation Mode	W_{net}	Q_{in}	Q_{out}	Thermal Efficiency
Heat engine	+	+	-	$\eta = \frac{W_{net}}{Q_{in}}$
Refrigerator	-	-	+	$COP = \frac{Q_{in}}{W_{net}}$
Heater	-	-	-	$COP = \frac{Q_{out}}{W_{net}}$
Accelerator	-	+	-	$COP = \frac{Q_{out}}{W_{net}}$

C. Thermal efficiency

In the heat engine mode, the efficiency of quantum engine, as shown in Table II, with $\eta < 1$. The coefficient of performance (COP) for other operation modes is also detailed in Table II. Given that COPs are typically greater than one, we introduce an alternative expression

$$\kappa = \frac{COP}{1 + COP}. \quad (8)$$

This new metric evaluates COP within a bounded range of $0 < \kappa < 1$, implying that as COP approaches 0, κ similarly trends toward 0, while κ approaches 1 as COP tends to infinity. Additionally, a $COP = 1$ corresponds to $\kappa = 0.5$. Consequently, the thermal efficiency for all operational modes can be defined within the range of 0 to 1, with 0 indicating the worst performance and 1

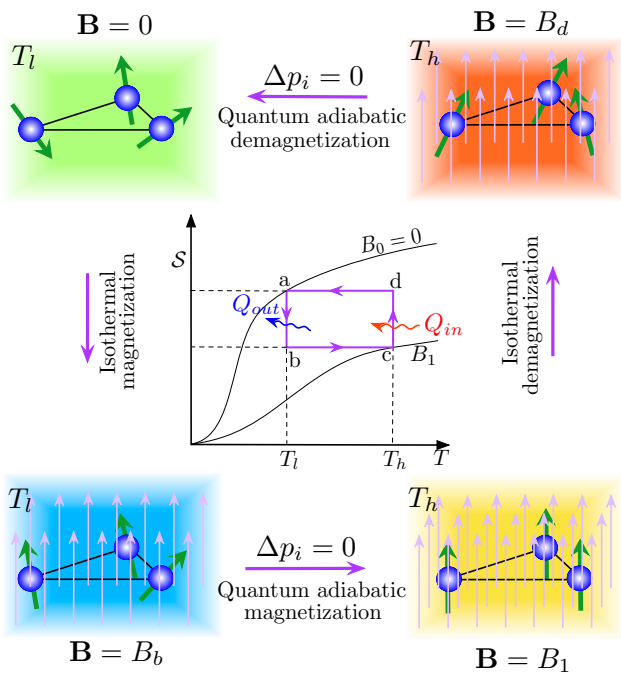


Figure 2. Schematic representation of Quantum Carnot machine cycle for Cu_3 -like compound. Magnetic field is turned on (B_1) or turned off ($B_0 = 0$).

the best. This definition is applicable to the refrigerator, heater, and accelerator, each described in Table II.

From now on, our discussion will focus on the $\text{Cu}_3 - \text{As}$ compound, as the $\text{Cu}_3 - \text{Sb}$ compound demonstrates similar characteristics, with parameters values closely comparable to those of $\text{Cu}_3 - \text{As}$, as shown in Table I.

III. QUANTUM CARNOT MACHINE

The quantum Carnot machine is a theoretical concept showing the highest efficiency possible for a heat engine. It's key for understanding how efficiently energy can be used in quantum systems like the Cu_3 -like compound. This idea is really useful in the field of quantum thermodynamics, helping us learn about how energy works at the quantum level.

According to Fig.2, we will describe all the steps of the Carnot cycle below. For simplicity, we will assume, without losing generality, that when the external magnetic field is increased, the spins try to align parallel to the external magnetic field. Although this is not the general rule, frustration can invert this process (see [52]). However, our analysis will still remain the same; the only change would be that instead of heat being observed, heat will be released or vice versa.

1. Isothermal magnetization process (a-b): The Cu_3 -like compound is placed in a isolated environment. When it comes into contact with a colder reservoir

at temperature T_l , the external magnetic field gradually increases, causing the Cu_3 -like compound to release heat to the cold reservoir,

$$Q_{ab} = T_l [\mathcal{S}(T_l, B_b) - \mathcal{S}(T_l, B_0)], \quad (9)$$

decreasing magnetic entropy and aligning the spins with the magnetic field. According to the quantum adiabatic condition $p_i(T_l, B_b) = p_i(T_h, B_1)$, which implies that $\mathcal{S}(T_l, B_b) = \mathcal{S}(T_h, B_1)$, thus we have

$$Q_{ab} = T_l [\mathcal{S}(T_h, B_1) - \mathcal{S}(T_l, B_0)]. \quad (10)$$

The change in internal energy in the isothermal process at low temperature T_l is

$$\Delta U_{ab} = U(T_l, B_b) - U(T_l, B_0), \quad (11)$$

and the corresponding work done is

$$W_{ab} = Q_{ab} - \Delta U_{ab}. \quad (12)$$

2. Adiabatic magnetization process (b-c): The system is again isolated, and the magnetic field is increased to B_1 aligning the spins. Since this process is a quantum adiabatic $Q_{bc} = 0$, and the temperature of the system rises to T_h . Therefore, the variation energy becomes

$$\Delta U_{bc} = U(T_h, B_1) - U(T_l, B_b), \quad (13)$$

and the respective work done is

$$W_{bc} = -\Delta U_{bc} = U(T_l, B_b) - U(T_h, B_1),$$

$$= \sum_{i=1}^8 [\varepsilon_i(B_b) p_i(T_l, B_b) - \varepsilon_i(B_1) p_i(T_h, B_1)], \quad (14)$$

using the quantum adiabatic condition $p_i(T_l, B_b) = p_i(T_h, B_1)$ the work done will become

$$W_{bc} = \sum_{i=1}^8 [\varepsilon_i(B_b) - \varepsilon_i(B_1)] p_i(T_h, B_1), \quad (15)$$

3. Isothermal demagnetization process (c-d). The system is brought into thermal contact with a hot reservoir at temperature T_h . The external magnetic field is gradually decreased. During this process, the Cu_3 -like absorb heat from the reservoir

$$Q_{cd} = T_h [\mathcal{S}(T_h, B_d) - \mathcal{S}(T_h, B_1)], \quad (16)$$

and their spin orientations become more disordered, increasing the magnetic entropy. Since the quantum adiabatic condition $p_i(T_h, B_d) = p_i(T_l, B_0)$, which implies that $\mathcal{S}(T_h, B_d) = \mathcal{S}(T_l, B_0)$, thus we have

$$Q_{cd} = T_h [\mathcal{S}(T_l, B_0) - \mathcal{S}(T_h, B_1)]. \quad (17)$$

The variation of internal energy at hot bath with temperature T_h is

$$\Delta U_{cd} = U(T_h, B_d) - U(T_h, B_1) \quad (18)$$

The corresponding work done is

$$W_{cd} = Q_{cd} - \Delta U_{cd}. \quad (19)$$

4. Adiabatic demagnetization process (d-a). The system is isolated from any heat reservoir, and the external magnetic field is further decreased. This process is adiabatic and the temperature of the system drops to T_l without any heat exchange $Q_{da} = 0$. And corresponding variation energy becomes

$$\Delta U_{da} = U(T_l, B_0) - U(T_h, B_d), \quad (20)$$

the work done is

$$W_{da} = -\Delta U_{da} = U(T_h, B_d) - U(T_l, B_0),$$

$$= \sum_{i=1}^8 [\varepsilon_i(B_d)p_i(T_h, B_d) - \varepsilon_i(B_0)p_i(T_l, B_0)], \quad (21)$$

using the quantum adiabatic condition $p_i(T_h, B_d) = p_i(T_l, B_0)$ the work done results in

$$W_{da} = \sum_{i=1}^8 [\varepsilon_i(B_1) - \varepsilon_i(B_d)] p_i(T_l, B_0), \quad (22)$$

Finally, the net work is given by

$$W_{net} = W_{ab} + W_{bc} + W_{cd} + W_{da} \quad (23)$$

or equivalently

$$W_{net} = Q_{ab} + Q_{cd}.$$

The heat absorbed and released are respectively $Q_{in} = Q_{ab}$ and $Q_{out} = Q_{cd}$.

Certainly, it is essential to consider the heat engine efficiency, denoted as η give by $\eta = 1 + Q_{out}/Q_{in} = 1 - T_l/T_h$. When the Carnot engine operates as a refrigerator, the COP becomes $COP = Q_{in}/W_{net} = \frac{T_h}{T_h - T_l}$. Obviously, for the Carnot engine, both thermal efficiencies are unaffected by the magnetic field.

In Fig. 3, we show the operational modes of the quantum Carnot cycle for a $\text{Cu}_3\text{-As}$ compound in the B_0 vs. B_1 plane. The green region indicates the heat engine mode, and the cyan region indicates the refrigerator mode. Panel (a) displays for cold reservoir $T_l = 0.5\text{K}$ and hot reservoir $T_h = 1\text{K}$. Assuming $B_0 = 0$, the system operates as a heat engine for $B_1 > 1.2$ and as a refrigerator at $B_1 \approx 4.7\text{T}$. The temperatures and magnetic fields values were chosen such that the MCE is enhanced[52]. The heat engine efficiency is $\eta = 0.5$ in the green region, with a refrigerator COP of 2. Panel (b) for $T_l = 0.7\text{K}$ and $T_h = 1\text{K}$ shows similar behavior, with refrigeration

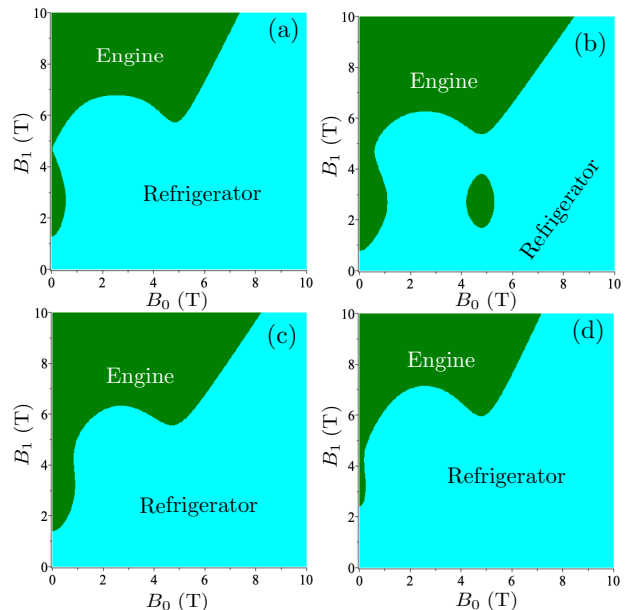


Figure 3. Operational modes of the quantum Carnot cycle for $\text{Cu}_3\text{-As}$ compound in the B_0 - B_1 plane. The green region operates as engine, while the cyan region operates as refrigerator. (a) For $T_l = 0.5\text{K}$ and $T_h = 1\text{K}$. (b) For $T_l = 0.7\text{K}$ and $T_h = 1\text{K}$. (c) For $T_l = 0.7\text{K}$ and $T_h = 1.5\text{K}$. (d) For $T_l = 1\text{K}$ and $T_h = 1.5\text{K}$.

around $B_1 \approx 4.7\text{T}$ and a small heat engine region at $B_0 \approx 5\text{T}$ and $B_1 \approx 3\text{T}$. The efficiency is $\eta = 0.3$, with a COP of 3.333. In panel (c) with ($T_l = 0.7\text{K}$, $T_h = 1.5\text{K}$), the small heat engine region disappears, but operation continues at $B_0 \approx 0\text{T}$ and $B_1 \approx 4.7\text{T}$. The efficiency is $\eta = 0.533$, with a COP of 1.875. Panel (d) with $T_l = 1\text{K}$ and $T_h = 1.5\text{K}$ resembles panel (a), with heat engine operation for $B_1 > 2.5\text{T}$, efficiency $\eta = 0.333$, while the COP for the refrigerator is $COP = 3$.

Another interesting analysis would involve examining the operational mode in the $B_0 - T_h$ plane, as illustrated in Fig.4. In Panel (a), we consider $T_l = 0.1\text{K}$ and $B_0 = 0$. The pink curve serves as the boundary between the two operational modes: heat engine and refrigerator. Whereas in panel (c), we present a density plot that indicates the thermal efficiency under the same conditions as in panel (a). Here, we observe that the refrigerator operation COP is consistently above 1, or equivalently, κ is greater than approximately 0.5. Meanwhile, the efficiency of the Carnot heat engine remains roughly above 0.8 in a vast region. As we increase the temperature T_h , the system becomes more efficient, leading roughly $\eta \approx 0.96$. Panel (b) shows a similar plot but assumes a fixed $T_l = 0.5\text{K}$ and $B_0 = 0$. Once again, the pink curve delineates the boundary between the heat engine and refrigerator operation modes. Essentially, we observe a similar behavior here, although the COP of the refrigerator consistently exceeds 1, or κ is approximately 0.6. Meanwhile, the efficiency of the heat engine at low T_h is inferior, and for higher temperatures, η becomes

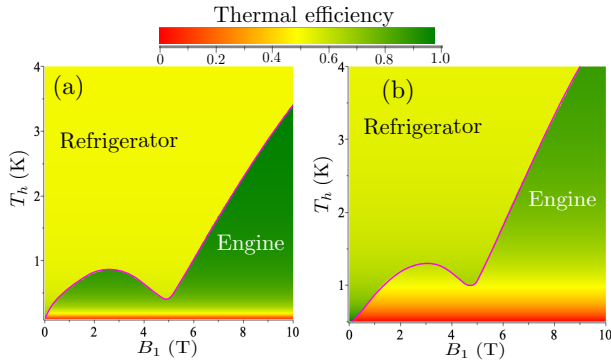


Figure 4. Operational modes of the quantum Carnot cycle for $\text{Cu}_3\text{-As}$ compound in the $B_1 - T_h$ plane. Below the pink curve operates as a heat engine, while above the curve operates as a refrigerator. (a) For $T_l = 0.1\text{K}$ and $B_0 = 0\text{T}$. (b) For $T_l = 0.5\text{K}$ and $B_0 = 0\text{T}$.

more efficient but remains lower than in panel (a). It is worth noting that for each operational mode, the thermal efficiency remains independent of the magnetic field B_1 .

Hence, comprehending the quantum Carnot engine of Cu_3 -like compounds is a crucial step in exploring quantum phenomena for practical technological progress.

IV. QUANTUM OTTO MACHINE

Now we will look at how a compound similar to Cu_3 could work as a quantum Otto machine as illustrated in Fig.5. This study is important for the field of quantum thermodynamics, as it offers insights into how Cu_3 -like quantum systems might be used for energy conversion. Understanding the quantum versions of classical thermodynamic processes can help us better manage energy at a tiny, microscopic scale.

1. Adiabatic magnetization process (a-b): In this process, the system isolates itself from the reservoir. The external magnetic field increases from B_0 to B_1 , aligning the spin orientation. No heat is transferred ($Q_{ab} = 0$), even as the temperature rises. Consequently, the change in energy is

$$\Delta U_{ab} = U(T_b, B_1) - U(T_l, B_0) \quad (24)$$

and the work done is

$$W_{ab} = -\Delta U_{ab} = U(T_l, B_0) - U(T_b, B_1),$$

$$= \sum_{i=1}^8 [\varepsilon_i(B_0)p_i(T_l, B_0) - \varepsilon_i(B_1)p_i(T_b, B_1)], \quad (25)$$

using the quantum adiabatic condition $p_i(T_b, B_1) = p_i(T_l, B_0)$, we can obtain

$$W_{ab} = \sum_{i=1}^8 [\varepsilon_i(B_0) - \varepsilon_i(B_1)] p_i(T_l, B_0). \quad (26)$$

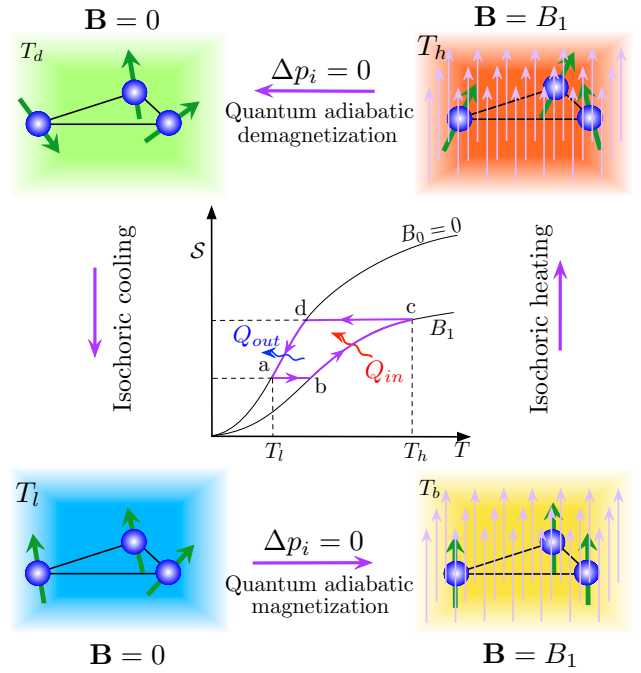


Figure 5. Schematic representation of Quantum Otto machine cycle for a Cu_3 -like compound. Magnetic field is turned on or turned off.

2. isochoric process (b-c): In this stage, the system comes into thermal contact with a hot reservoir, and the temperature increases while keeping the magnetic field constant. No work is done, $W_{bc} = 0$. Consequently, the system absorbs heat, which is given by

$$Q_{bc} = \Delta U_{bc} = U(T_h, B_1) - U(T_b, B_1),$$

$$= \sum_{i=1}^8 \varepsilon_i(B_1) [p_i(T_h, B_1) - p_i(T_b, B_1)]. \quad (27)$$

Taking into account the quantum adiabatic condition, $p_i(T_b, B_1) = p_i(T_l, B_0)$, thus the heat becomes

$$Q_{bc} = \sum_{i=1}^8 \varepsilon_i(B_1) [p_i(T_h, B_1) - p_i(T_l, B_0)]. \quad (28)$$

3. Adiabatic demagnetization process (c-d): In this stage, the Cu_3 -like system is once again isolated from the reservoir, and the external magnetic field decreases adiabatically ($Q_{cd} = 0$), causing the system to cool. The corresponding change energy reads

$$\Delta U_{cd} = U(T_d, B_0) - U(T_h, B_1), \quad (29)$$

and the work done is .

$$W_{bc} = -\Delta U_{bc} = U(T_h, B_1) - U(T_d, B_0),$$

$$= \sum_{i=1}^8 [\varepsilon_i(B_1)p_i(T_h, B_1) - \varepsilon_i(B_0)p_i(T_d, B_0)]. \quad (30)$$

considering the quantum adiabatic condition where $p_i(T_d, B_0) = p_i(T_h, B_1)$, we have

$$W_{bc} = \sum_{i=1}^8 [\varepsilon_i(B_1) - \varepsilon_i(B_0)] p_i(T_h, B_1). \quad (31)$$

4. isochoric process (d-a): In this process, the system comes into contact with a cold environment, gradually lowering its temperature. Since there is no change in the magnetic field, no work is done ($W_{da} = 0$). The heat released to the environment is given by

$$\begin{aligned} Q_{da} &= \Delta U_{da} = U(T_l, B_0) - U(T_d, B_0), \\ &= \sum_{i=1}^8 \varepsilon_i(B_0) [p_i(T_l, B_0) - p_i(T_d, B_0)]. \end{aligned} \quad (32)$$

Considering the quantum adiabatic condition given by $p_i(T_d, B_0) = p_i(T_h, B_1)$, we obtain

$$Q_{cd} = \sum_{i=1}^8 \varepsilon_i(B_0) [p_i(T_l, B_0) - p_i(T_h, B_1)]. \quad (33)$$

Finally, the total work done is given by

$$W_{net} = \sum_{i=1}^8 [\varepsilon_i(B_1) - \varepsilon_i(B_0)] [p_i(T_h, B_1) - p_i(T_l, B_0)]. \quad (34)$$

In Fig. 6, we present the operational modes of the quantum Otto cycle for a $\text{Cu}_3\text{-As}$ compound in the $B_0 - B_1$ plane. The color-coded regions signify different modes of operation: the green region represents the engine mode, the cyan region represents the refrigerator mode, the yellow region corresponds to the heater mode, and the red region indicates the accelerator mode. In Panel (a), we consider the case with $T_l = 0.5\text{K}$ and $T_h = 1\text{K}$, the choice of these parameters is related to the MCE enhancement. Just to explore the MCE, we assume conveniently B_0 is approximately 0.1T . Notably, the system exhibits peculiar behavior in the range of $2.2\text{T} \lesssim B_1 \lesssim 3.8\text{T}$, where it functions as a refrigerator. However, at $B_1 \approx 4\text{T}$, where the MCE is significantly enhanced, the system operates as a thermal accelerator. For $B_0 > B_1$, the system predominantly acts as a thermal accelerator, while for $B_1 > B_0$, it exhibits four operation modes. Specifically, for $B_1 \gtrsim B_0$, the system serves as a heat engine, and where the MCE is enhanced, it behaves as an accelerator. In Panel (b), with $T_l = 0.7\text{K}$ and $T_h = 1\text{K}$, we observe similar behavior. Although in this case, the $\text{Cu}_3\text{-As}$ compound could work as a refrigerator at $B_1 \approx 1\text{T}$. However, a small region appears as a refrigerator at $B_0 \approx 5\text{T}$, surrounded by a heater operation mode. In Panel (c), for $T_l = 0.7\text{K}$ and $T_h = 1.5\text{K}$, the region where the system operates as a refrigerator and heater at $B_0 \approx 5\text{T}$ and $B_1 \approx 3\text{T}$ disappears. However, for $B_0 \approx 0.1\text{T}$ and $B_1 \approx 3\text{T}$, the system continues

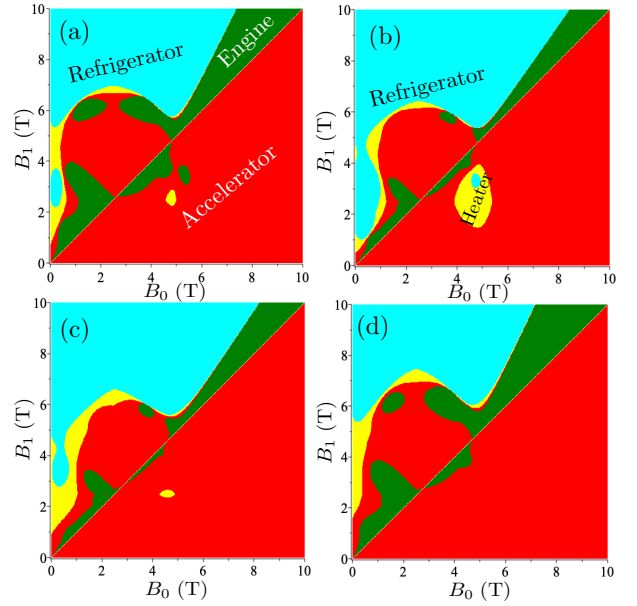


Figure 6. Operational modes of the quantum Otto cycle for $\text{Cu}_3\text{-As}$ compound in the $B_0 - B_1$ plane. In green region operates as an engine, in cyan region operates as refrigerator, the yellow region operates as heater, and in red region operates accelerator. (a) For $T_l = 0.5\text{K}$ and $T_h = 1\text{K}$. (b) For $T_l = 0.7\text{K}$ and $T_h = 1\text{K}$. (c) For $T_l = 0.7\text{K}$ and $T_h = 1.5\text{K}$. (d) For $T_l = 1\text{K}$ and $T_h = 1.5\text{K}$.

to operate as a refrigerator. Similarly, in Panel (d), for $T_l = 1\text{K}$ and $T_h = 1.5\text{K}$, the behavior is somewhat akin to panel (a), although for $B_0 = 0$ and $B_1 \gtrsim 5\text{T}$, it operates as a refrigerator.

In contrast to the Carnot engine discussed in the previous section, the Otto engine can operate in four distinct modes: heat engine, refrigerator, heater, and accelerator.

For engine heat, we use η to represent thermal efficiencies, while for different COPs for the refrigerator, heater, and accelerator, we employ the eq. (8). This information is presented in Fig.7, using the same parameter set as in Fig.3. In this representation, regions shaded in red indicate poor efficiency, green regions correspond to the best efficiency, and yellow regions indicate efficiency values of $\eta = 0.5$. Similarly, for COPs, $\kappa = 0.5$ corresponds to $COP = 1$. Broadly, we observe that $\kappa \gtrsim 0.5$ or $COP \gtrsim 1$, while for heat engines, $\eta \lesssim 0.5$. This essentially means that no heat engine achieves an efficiency greater than $\eta > 0.5$.

Additionally, we can analyze the quantum operational modes as functions of the hot temperature T_h and magnetic field B_1 , assuming $B_0 = 0\text{T}$. In contrast to the Carnot engine, thermal efficiency now depends on the magnetic fields B_0 and B_1 , as well as the temperatures T_l and T_h . In Fig.8, Panel (a) illustrates the operational modes of the quantum Otto cycle for a $\text{Cu}_3\text{-As}$ compound in the $B_1 - T_h$ plane, assuming fixed values of $T_l = 0.1\text{K}$ and $B_0 = 0$. Under these conditions, we observe all four operational modes: engine (green), refrigerator (cyan),

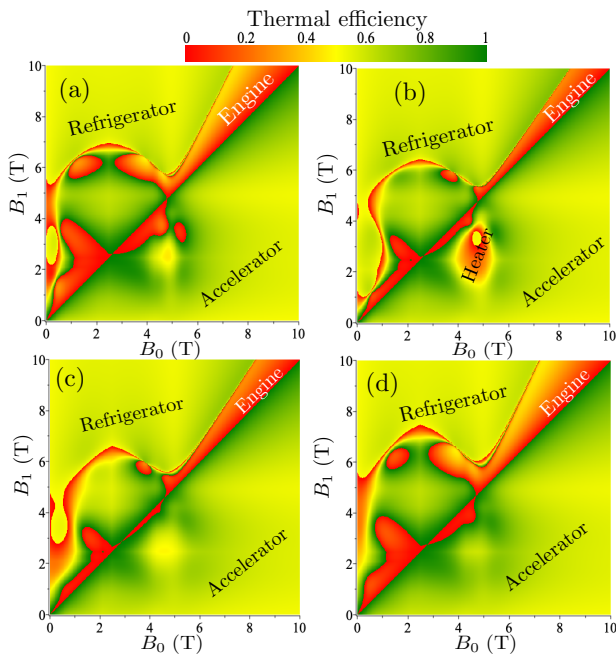


Figure 7. Thermal efficiency of the quantum Otto cycle for $\text{Cu}_3\text{-As}$ compound in the B_0 - B_1 plane. The cycle is evaluated under varying cold (T_l) and hot (T_h) temperature conditions: (a) For $T_l = 0.5$ and $T_h = 1$. (b) For $T_l = 0.7$ and $T_h = 1$. (c) For $T_l = 0.7$ and $T_h = 1.5$. (d) For $T_l = 1$ and $T_h = 1.5$.

heater (yellow), and accelerator (red). Panel (b) presents a similar plot but assumes $T_l = 0.5\text{K}$ and $B_0 = 0\text{T}$. It demonstrates that at lower temperatures, the system can function as a refrigerator, although this region significantly decreases for lower T_h values. Conversely, for higher temperatures, the system tends to operate as a heat engine. In panels (c-d), we depict the thermal efficiency under the same conditions as in panels (a-b), respectively. For thermal efficiency, we use η for the heat engine and κ for the refrigerator, heater, and accelerator, as detailed in Table II. Here, we can observe that thermal efficiency depends on T_h and B_1 . The COP of the refrigerator is roughly around $COP = 1$ or $\kappa = 0.5$, while the efficiency of the heat engine is approximately $\eta \sim 0.2$. The COP for the heater is also quite small. However, the efficiency of the thermal accelerator is notably strong, approaching $\kappa \rightarrow 1$.

Hence, the $\text{Cu}_3\text{-As}$ compound may offer certain advantages, mainly in low-temperature region around MCE is relevant, around $B_1 \sim 4.7\text{T}$, and for temperature $T_h \gtrsim 2\text{K}$, the heat engine operates with high efficiency roughly around $\eta \sim 0.5$.

As technology increasingly miniaturizes and ventures into the quantum domain, insights from the quantum Otto engine could lead to the development of highly efficient, novel quantum technologies and devices, with wide-ranging applications from computing to material science.

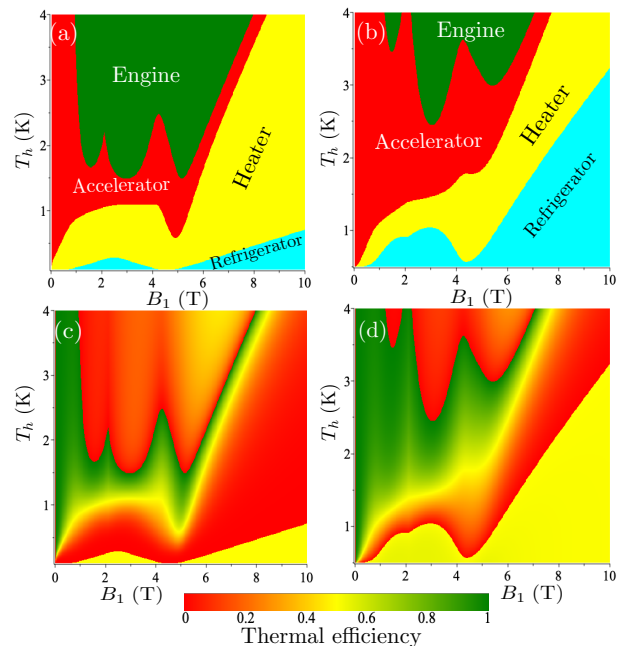


Figure 8. (a) Operation mode of the quantum Otto cycle for $\text{Cu}_3\text{-As}$ compound in the plane $B_1 - T_h$, for $T_l = 0.1$ and $B_0 = 0$. (b) For $T_l = 0.5$ and $B_0 = 0$. (c-d) Thermal efficiency under the same condition to (a-b) respectively.

V. QUANTUM STIRLING MACHINE

Finally, we consider how Cu_3 -like compound could work as a quantum Stirling machine (see Fig. 9) which represents a relevant stride in the field of quantum thermodynamics, offering insights into the manipulation and potential applicability of quantum Cu_3 -like systems for energy conversion. By understanding the quantum mechanical counterparts of classical thermodynamic processes, could help the energy management at microscopic scales.

1. Isothermal magnetization process (a-b). In this process the temperature is hold constant T_l , and increases gradually the magnetic field up to B_1 , consequently the magnetic entropy decreases. The internal energy variation is given by

$$\Delta U_{ab} = U(T_l, B_1) - U(T_l, B_0), \quad (35)$$

and the heat released to the environment is

$$Q_{ab} = T_l [\mathcal{S}(T_l, B_1) - \mathcal{S}(T_l, B_0)]. \quad (36)$$

Therefore, the Cu_3 -like system work realized in this process becomes

$$W_{ab} = Q_{ab} - \Delta U_{ab}. \quad (37)$$

2. isochoric process (b-c). In this process no work is realized by the compound, because the magnetic

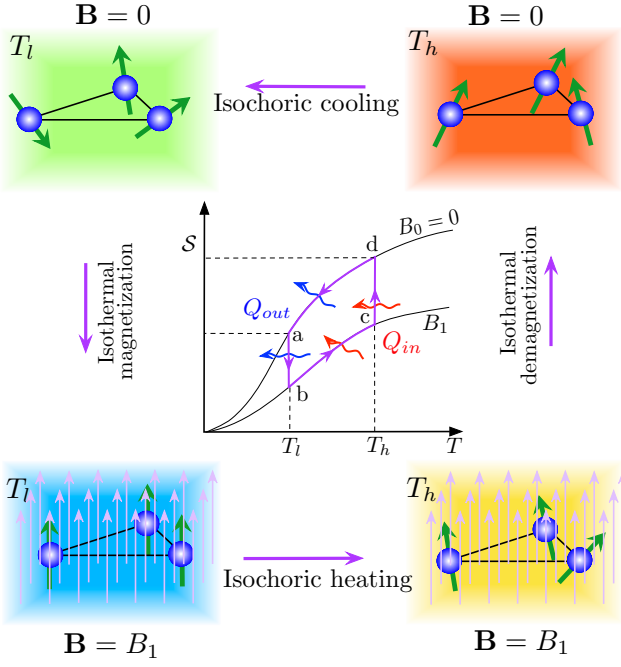


Figure 9. Schematic representation of Quantum Stirling machine cycle for a Cu_3 -like compound. Magnetic field is turned on or turned off.

field holds constant $W_{bc} = 0$. However, the temperature of the system increases to T_h increasing the magnetic entropy and spins alignments becoming more erratic, consequently the system absorb heat from the reservoir, which is given by

$$Q_{bc} = \Delta U_{bc} = U(T_h, B_1) - U(T_l, B_1),$$

$$= \sum_{i=1}^8 \varepsilon_i(B_1) [p_i(T_h, B_1) - p_i(T_l, B_1)]. \quad (38)$$

3. Isothermal process (c-d). In this process again the temperature remains constant at T_h , while external magnetic field is decreased absorbing heat from the reservoir

$$Q_{cd} = T_h [\mathcal{S}(T_h, B_0) - \mathcal{S}(T_h, B_1)], \quad (39)$$

when magnetic field is decreased the spin alignment start disarranging, leading to higher entropy. Therefore, the work realized in this process becomes

$$W_{cd} = Q_{cd} - \Delta U_{cd}. \quad (40)$$

The variation of internal energy at hot bath with temperature T_h is

$$\Delta U_{cd} = U(T_h, B_0) - U(T_h, B_1). \quad (41)$$

4. isochoric process (d-a). Here the Cu_3 -like system is placed in contact with cold bath consequently decreasing the magnetic entropy and then the temperature of the system also decreases, but since there

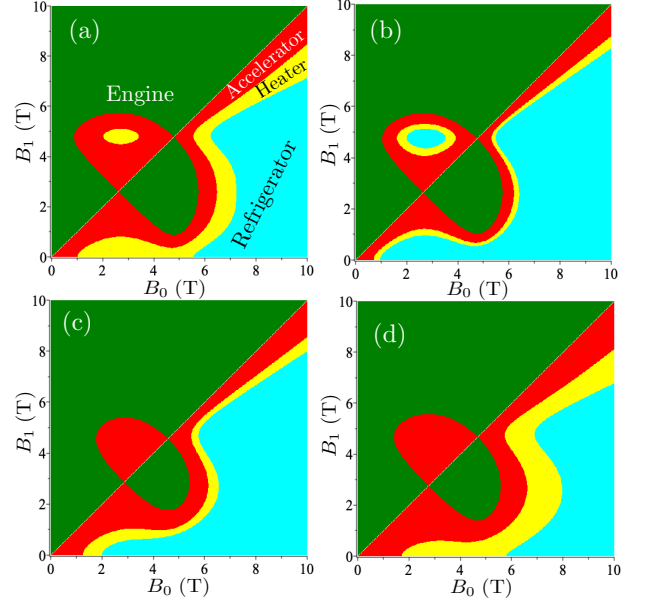


Figure 10. Operational modes of the quantum Stirling cycle for Cu_3 -As compound in the B_0 - B_1 plane. In green region operates as an engine, in cyan region operates as a refrigerator, the yellow region operates as a heater, and in red region operates accelerator. (a) For $T_l = 0.5\text{K}$ and $T_h = 1\text{K}$. (b) For $T_l = 0.7\text{K}$ and $T_h = 1\text{K}$. (c) For $T_l = 0.7\text{K}$ and $T_h = 1.5\text{K}$. (d) For $T_l = 1\text{K}$ and $T_h = 1.5\text{K}$.

is no change of magnetic field, then no work is realized $W_{da} = 0$. Thus the heat released to the cold bath by the system is given by

$$Q_{da} = \Delta U_{da} = U(T_l, B_0) - U(T_h, B_0),$$

$$= \sum_{i=1}^8 \varepsilon_i(B_0) [p_i(T_l, B_0) - p_i(T_h, B_0)]. \quad (42)$$

The total work done can be expressed as a sum of the all works done

$$W_{net} = W_{ab} + W_{cd}, \quad (43)$$

whereas the heat absorbed by the system becomes

$$Q_{in} = Q_{bc} + Q_{cd} \quad (44)$$

and the heat released to the cold bath is

$$Q_{out} = Q_{da} + Q_{ab}. \quad (45)$$

In Fig.10, we present the quantum operational modes of the Stirling cycle for an engine using a Cu_3 -As compound in the B_0 - B_1 plane. Panel (a) illustrates this for fixed temperatures $T_l = 0.5\text{K}$ and $T_h = 1\text{K}$. It is clear that when $B_1 > B_0$, the system mainly operates as a heat engine. Conversely, when $B_1 < B_0$, the system functions

as a refrigerator. Interestingly, around $B_0 \sim 4.5\text{T}$ and $B_1 \sim 3\text{T}$, there is a region where it operates as a heat engine. In contrast, around $B_0 \sim 3\text{T}$ and $B_1 \sim 4.5\text{T}$, the system functions as an accelerator. There is even a small region at $B_0 \sim 3\text{T}$ and $B_1 \sim 5\text{T}$ where it operates as a heater. Additionally, between these two main operational modes, there are regions where the heater and thermal accelerator modes occur, particularly when $B_1 \lesssim B_0$. Panel (b) depicts the scenario for $T_l = 0.7\text{K}$ and $T_h = 1\text{K}$, showing a similar pattern to panel (a). The main difference is that the heater operation mode is significantly reduced. However, at $B_0 \sim 3\text{T}$ and $B_1 \sim 5$, the system operates as a refrigerator, surrounded by the heater operation mode. Moreover, for $B_0 \sim 4.5\text{T}$ and $B_1 \lesssim 1\text{T}$, the system acts as a refrigerator. In Panel (c), we plot the results for $T_l = 0.7\text{K}$ and $T_h = 1.5\text{K}$, which is again similar to (b). However, there are no heater or refrigerator modes at $B_0 \sim 3\text{T}$ and $B_1 \sim 5$, though the accelerator mode still remains at $B_0 \sim 4.5\text{T}$ and $B_1 \lesssim 1\text{T}$. Finally, Panel (d) presents results for a different set of parameters, $T_l = 1\text{K}$ and $T_h = 1.5\text{K}$. Here, we observe wider regions for the heater and accelerator modes, but the inversion operation mode still occurs at $B_0 \sim 3\text{T}$ and $B_1 \sim 4.5\text{T}$, and vice versa.

Our next analysis focuses on the thermal efficiency of the operating modes of the quantum Stirling engine. To conveniently present this, we display it in Fig.11, assuming the conditions considered in Fig.10. We calculate the thermal efficiency using the values provided in Table II and Eq.(8). When the Stirling machine operates as a heat engine, the efficiency is notably $\eta \lesssim 0.5$ in the vast region where it functions. This efficiency is even higher in panel (a) for $B_1 \gtrsim 5\text{T}$ and when $B_1 > B_0$. On the other hand, when it operates as a refrigerator, the thermal efficiency is slightly above $\kappa \gtrsim 0.5$ or $COP \gtrsim 1$, showing better efficiency in panels (b-c). When the system works as a heater, the thermal efficiency is clearly below $\kappa < 0.5$ in most of the region where it operates. Finally, when the system functions as a thermal accelerator, the corresponding efficiency becomes considerably high.

It is worth noting that in the region where the magnetocaloric effect is more prominent, the quantum operation mode undergoes a type of inversion. Similar to the Otto machine, the Stirling machine has four operational modes: heat engine, refrigerator, heater, and accelerator. The quantum Stirling engine could serve as a prototype for elucidating the fundamental principles of quantum heat engines and potential technological application[54].

VI. CONCLUSION

This paper investigates the $\text{Cu}_3 - X$ ($X = \text{As}, \text{Sb}$) anti-ferromagnetic spin system with a slightly distorted equilateral triangular configuration. Using the Heisenberg model on a triangular lattice, it incorporates exchange interactions, Dzyaloshinskii-Moriya interaction, g -factors,

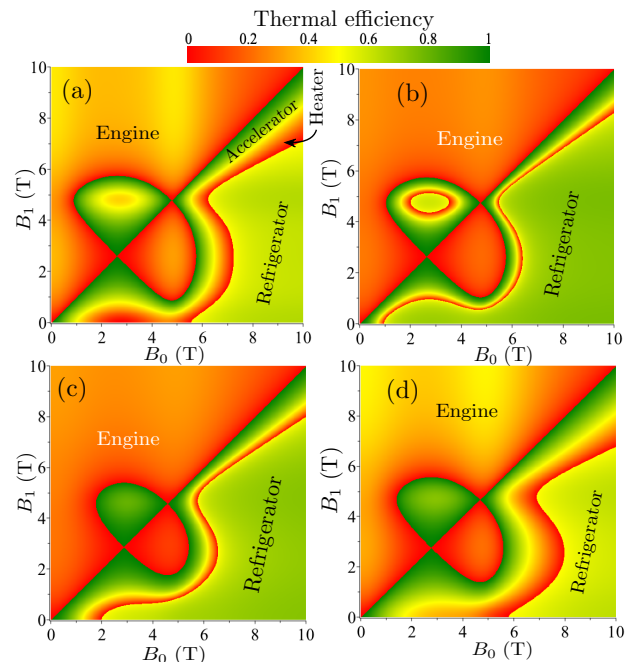


Figure 11. Thermal efficiency of the quantum Stirling cycle for $\text{Cu}_3\text{-As}$ compound in the B_0 - B_1 plane. The cycle is evaluated under varying cold (T_l) and hot (T_h) temperature conditions: (a) For $T_l = 0.5$ and $T_h = 1$. (b) For $T_l = 0.7$ and $T_h = 1$. (c) For $T_l = 0.7$ and $T_h = 1.5$. (d) For $T_l = 1$ and $T_h = 1.5$.

and external magnetic fields to represent system properties as highlighted in prior research [36, 38, 39]. The significance of the Cu_3 -like system, driven by its fundamental properties, has grown due to potential applications in spintronics, nanotechnology, and biomedicine. The MCE in $\text{Cu}_3 - X$, especially at low temperatures (around $T \approx 1\text{K}$) under perpendicular magnetic fields ($\sim 5\text{T}$), is also analyzed [52]

The MCE impact on quantum machine operation and efficiency is significant. We explored the Carnot, Otto, and Stirling machines within a Cu_3 -like system as the working substance, focusing on how external magnetic fields and temperature affect their performance assuming reversible process. The Carnot machine operates as a heat engine for $B_1 \lesssim B_0$ and as a refrigerator for $B_1 \gtrsim B_0$, with a shift in mode near the MCE. The Otto machine is versatile, mainly functioning as a thermal accelerator for $B_1 < B_0$ and as a refrigerator for $B_1 > B_0$, with a small region where it acts as a heat engine and heater. The Stirling machine alternates between a heat engine and thermal accelerator near the MCE, operating primarily as a heat engine for $B_1 > B_0$ and as a refrigerator for $B_1 < B_0$. We also evaluated their thermal efficiencies for each machines. This study enhances the understanding of quantum heat machines, especially in low-temperature regimes where the MCE is crucial, offering insights into practical applications of the $\text{Cu}_3 - X$ system in quantum thermodynamics. Although our anal-

ysis focused solely on the compound $\text{Cu}_3\text{-As}$, the second compound $\text{Cu}_3\text{-Sb}$ will also exhibit similar behavior for Carnot, Otto, and Stirling machines, with no relevant changes worth commenting on, as analyzed in Ref.[52]. We did not include any plots here to avoid repetitive behavior.

Future research could focus on optimizing quantum machines using Cu_3 -like systems through material tuning, analyzing non-ideal quantum conditions, and expanding applications in quantum refrigeration, assuming

non-reversible quantum machines.

ACKNOWLEDGMENTS

O. R. and M. Rojas thank CNPq and FAPEMIG for partial financial support. M. Rojas acknowledges FAPEMIG Grant APQ-02226-22.

-
- [1] H. T. Quan, Y. X. Liu, C. P. Sun, F. Nori, *Phys. Rev. E*, **76**, 031105 (2007).
- [2] N. M. Myers, O. Abah, S. Deffner, *AVS Quantum Sci.* **4**, 027101 (2022).
- [3] R. Kosloff, *J. Chem. Phys.* **80**, 1625 (1984).
- [4] R. Alicki, *J. Phys. A: Math. Gen.* **12**, L103 (1979).
- [5] T. Zhang, W.-T. Liu, P.-X. Chen, Ch.-Z. Li, *Phys. Rev. A* **75**, 062102 (2007).
- [6] X. He, J. H. J. Zheng, *Physica A* **391**, 6594 (2012).
- [7] R. Kosloff, A. Levy, *Ann. Rev. Phys. Chem.* **65**, 365 (2014).
- [8] A. Insinga, B. Andresen, P. Salamon, *Phys. Rev. E* **94**, 012119 (2016).
- [9] Y. Rezek, R. Kosloff, *New J. Phys.* **8**, 83 (2006).
- [10] M. Josefsson, A. Svilans, A. M. Burke, E. A. Hoffmann, S. Fahlvik, C. Thelander, M. Leijnse, H. Linke, *Nat. Nanotechnol.* **13**, 920 (2018)
- [11] J. L. D. de Oliveira, M. Rojas, C. Filgueiras, *Phys. Rev. E* **104**, 014149 (2021)
- [12] M. L. Bera, M. Lewenstein, M. N. Bera, *npj Quantum Information* **7**, 4430 (2021)
- [13] S. Çakmak, F. Altintas, *Quantum Information Proc.* **19**, 248 (2020)
- [14] F. J. Peña, O. Negrete, N. Cortés, P. Vargas, *Entropy* **22**, 755 (2020)
- [15] D. Gelbwaser-Klimovsky, A. Bylinskii, D. Gangloff, R. Islam, A. Aspuru-Guzik, V. Vuletic, *Phys. Rev. Lett.* **120**, 170601 (2018)
- [16] X.-L. Huang, X.-Y. Viu, X.-M. Viu, X.-X. Yi, *Eur. Phys. J. D* **68**, 32 (2014)
- [17] S. Çakmak, *J. Opt. Soc. Am. B* **39**, 1209 (2022)
- [18] C. Cruz, H.-R. Rastegar-Sedehi, M. Anka, T. R. de Oliveira, M. Reis, *Quant. Science Tech.* **8**, 035010 (2023)
- [19] T. R. de Oliveira, D. Jonathan, *Phys. Rev. E*, **104**, 044133 (2021).
- [20] A. El Makouri, A. Slaoui, M. Daoud, *J. Phys. B: At. Mol. Opt. Phys.* **56**, 085501 (2023).
- [21] Y. Yin, L. Chen, F. Wu, Y. Ge, *Physica A* **547**, 123856 (2020)
- [22] M. Y. Abd-Rabbou, A. ur Rahman, M. A. Yurischev, S. Haddadi, *Phys. Rev. E* **108**, 034106 (2023)
- [23] M. Asadian, S. Ahadpour, F. Mirmasoudi, *Sci. Rep.* **12**, 7081 (2022)
- [24] J. Z. He, J. C. Chen, B. Hua, *Phys. Rev. E* **65**, 036145 (2002).
- [25] C. M. Bender, D. C. Body, B. K. Meister, *J. Phys A* **33**, 4427 (2000)
- [26] E. Aydinger, S. D. Han, *Physica A*, **509**, 766 (2018).
- [27] K. Klinar, M.M. Rojo, Z. Kutnjak, A. Kitanovski, *J. Appl. Phys.* **127**, 234101 (2020)
- [28] V. Chaudhary, Z. Wang, A. Ray, I. Sridhar, R.V. Ramanujan, *J. Phys. D* **50**, 03LT03 (2017)
- [29] M.S. Pattanaik, S.K. Cheekati, V.B. Varma, R.V. Ramanujan, *App. Therm. Eng.* **201**, 117777 (2022)
- [30] U. Sen, S. Chatterjee, S. Sen, M. K. Tiwari, A. Mukhopadhyay, R. Ganguly, *J. Magn. Magn. Mater.* **421**, 165 (2017)
- [31] M. Qian, X. Zhang, L. Wei, P. Martin, J. Sun, L. Geng, T. B. Scott, H.-X. Peng, *Scientific Reports* **8**, 16574 (2018)
- [32] D.N. Ba, L. Becerra, N. Casaretto, J.E. Duvauchelle, M. Marangolo, S. Ahmim, M. Almanza, M. LoBue, *AIP Adv.* **10**, 035110 (2020).
- [33] D.N. Ba, Y.L. Zheng, L. Becerra, M. Marangolo, M. Almanza, M. LoBue, *Phys. Rev. Appl.* **15**, 064045 (2021)
- [34] X.L. Liu, Y.F. Zhang, Y.Y. Wang, W.J. Zhu, G.L. Li, X.W. Ma, Y.H. Zhang, S.Z. Chen, S. Tiwari, K.J. Shi, S.W. Zhang, H.M. Fan, Y.X. Zhao, X.J. Liang, *Theranostics* **10**, 3793 (2020)
- [35] J.B. Li, Y. Qu, J. Ren, W.Z. Yuan, D.L. Shi, *Nanotechnology* **23**, 505706 (2012)
- [36] K.-Y. Choi, Y. H. Matsuda and H. Nojiri, *Phys. Rev. Lett.* **96**, 107202 (2006)
- [37] M. Trif, F. Troiani, D. Stepanenko, and D. Loss, *Rev. Lett.* **101**, 217201 (2008)
- [38] K.-Y. Choi, N. S. Dalal, A. P. Reyes, P.L. Kuhns, Y. H. Matsuda, H. Hojiri, S. S. Mal and U. Kortz, *Phys. Rev. B* **77**, 024406 (2008)
- [39] K.-Y. Choi, Z. Wang, H. Nojiri, J. van Tol, P. Kumar, P. Lemmens, B. S. Bassil, U. Kortz, and N. S. Dalal, *Phys. Rev. Lett.* **108**, 067206 (2012)
- [40] E. T. Spielberg, A. Gilb, D. Plaul, D. Geibig, D. Hornig, D. Schuch, A. Buchholz, A. Ardavan, W. Plass, *Inorg. Chem.* **54**, 3432 (2015)
- [41] M. I. Belinsky, *Inorg. Chem.* **55**, 4091 (2016)
- [42] J. Robert, N. Parizel, P. Turek, A. K. Boudalis, *Phys. Chem. Phys.* **21**, 19575 (2019)
- [43] A. K. Boudalis, *Chem. Eur. J.* **27**, 7022 (2021)
- [44] A. C. Stowe, S. Nellutla, N. S. Dalal, U. Kortz, *Eur. J. Inorg. Chem.* **2004**, 3792 (2004)
- [45] U. Kortz, S. Nellutla, A. C. Stowe, N. S. Dalal, J. van Tol, B. S. Bassil, *Inorg. Chem.* **43**, 144 (2004)
- [46] T. Yamase, E. Ishikawa, K. Fukaya, H. Nojiri, T. Taniguchi, T. Atake, *Inorg. Chem.* **43**, 8150 (2004)
- [47] M.-A. Bouammali, N. Suaud, N. Guihéry, R. Maurice, *Inorg. Chem.* **61**, 12138 (2022)
- [48] P. Kowalewska, K. Szałowski, *J. Magn. Magn. Mater.* **496**, 165933 (2020)

- [49] K. Karlova, J. Strečka, J. Richter, *J. Phys.: Condens. Matter* **29**, 125802 (2017)
- [50] J. Torrico, J. A. Plascak, *Phys. Rev. E* **102**, 062116 (2020)
- [51] J. Torrico, J. A. Plascak, *J. Magn. Magn. Mater.* **552**, 169151 (2022)
- [52] G. A. Antonio, J. Torrico, A. S. da Mata, S. M. de Souza, O. Rojas, *Phys. Rev. B* **108**, 134415 (2023)
- [53] H. T. Quan, P. Zhang, C. P. Sun, *Phys. Rev. E* **72**, 056110 (2005).
- [54] D. Das, G. Thomas, A. N. Jordan, *Phys. Rev. A* **108**, 012220 (2023).